Deterministic Ultracold Ion Source Targeting the Heisenberg Limit

W. Schnitzler,[1] N. M. Linke,[1] R. Fickler,[1] J. Meijer,[2] F. Schmidt-Kaler,[1] and K. Singer[1,*]

[1]*Institut für Quanteninformationsverarbeitung, Universität Ulm, Albert-Einstein-Allee 11, 89081 Ulm, Germany*[†]

[2]*RUBION, Ruhr-Universität Bochum, 44780 Bochum, Germany*

(Received 26 September 2008; revised manuscript received 2 December 2008; published 19 February 2009)

The major challenges to fabricate quantum processors and future nano-solid-state devices are material modification techniques with nanometer resolution and suppression of statistical fluctuations of dopants or qubit carriers. Based on a segmented ion trap with mK laser-cooled ions we have realized a deterministic single-ion source which could operate with a huge range of sympathetically cooled ion species, isotopes or ionic molecules. We have deterministically extracted a predetermined number of ions on demand and have measured a longitudinal velocity uncertainty of 6.3 m/s and a spatial beam divergence of 600 μrad. We show in numerical simulations that if the ions are cooled to the motional ground state (Heisenberg limit) nanometer spatial resolution can be achieved.

DOI: 10.1103/PhysRevLett.102.070501 PACS numbers: 03.67.−a, 29.25.Ni, 81.16.Rf, 85.40.Ry

The miniaturization of semiconductor devices has reached length scales of a few tens of nanometers, where statistical Poissonian fluctuations of the number of doping atoms in a single transistor significantly affect the characteristic properties, e.g., gate voltage or current amplification [1]. Further miniaturization will even cause statistical device failure. Particularly fatal are statistical dopant fluctuations for a future solid state quantum processor based on single implanted qubit carriers like color centers in diamond or phosphorous dopants in silicon [2–5]. So far, the only known methods to control the number of dopants utilize statistical thermal sources followed by a postdetection of the implantation event, either by the observation of Auger electrons, photoluminescence, phonons, the generation of electron-hole pairs, or changes in the conductance of field effect transistors [6–10]. To make the detection of such an event successful the methods require either highly charged ions or high implantation energies which, as a down side, generate defects in the host material. In these systems resolutions of less than 10 nm are achieved by means of masks and apertures shielding the substrate from incident ions and leading to compulsory losses of dopants. Another fabrication method, specific for Si surfaces, uses hydrogen terminated surfaces structured with the tip of a tunneling microscope, followed by a chemical reactive surface binding of doping atoms [11–15]. With this technique sub-nm resolution can be achieved but the applicability is mainly limited to specific substrates and impurities in the background gas can cause severe impairment.

Here, we present the experimental proof of a novel ultracold ion source which can be used for the deterministic implantation of a predetermined number of single ions [16]. Our technique is based on a segmented linear Paul trap with laser-cooled $^{40}Ca^{+}$ ions similar to setups used for scalable quantum information processing with ions [17]. Additionally loaded doping ions of different elements or ionic molecules cannot be directly laser cooled but could be sympathetically cooled by $^{40}Ca^{+}$ ions. Although invisible to the laser light they are still identified [18,19] and counted by exciting collective vibrational modes. Our segmented ion trap allows for the separation of the cooling ion from the dopant ion, which is finally extracted by a tailored electric field. The implantation method is in principle independent of the dopant species and the target substrate. For 2 mK laser-cooled ions accelerated to 80 eV the measured longitudinal velocity distribution shows a 1σ spread of 6.3(6) m/s [20] and a spatial 1σ-spot radius of $83(^{+8}_{-3})$ μm at a distance of 257 mm (beam divergence: 600 μrad). These properties reduce chromatic and spherical aberration of any focusing ion optics. The resolution of our system is thereby not enforced by additional masks or apertures but is an intrinsic property of our setup.

The core of the experimental setup is a Paul trap—a universal tool for trapping charged particles such as atomic and molecular ions or charged clusters using a combination of static (dc) and alternating (rf) electric fields. A pseudopotential of a few eV depth is generated with a properly chosen rf amplitude and frequency Ω.

For our application it is necessary that the ions arrange as a linear crystal such that they can be identified and counted using laser induced fluorescence. During the extraction we apply voltages to additional dc segments tailoring the axial potential. In a conventional linear segmented Paul trap this would lead to a loss of the radial confinement because the applied extraction potential exceeds the radial pseudopotential. We have developed a special design of our trap, in which the ions are radially guided even during the axial extraction. Our trap consists of four copper plated polyimide blades of 410 μm thickness and 65 mm length which are arranged in a x-shaped manner [21] (see Fig. 1 for a schematic view). The rf is applied to the inner front faces of two opposing blades; the front faces of both other blades are grounded. The distance between inner front faces of opposing blades is 2 mm. dc voltages are applied to eight segments of 0.7 mm width which are placed on the top and bottom areas of all four blades. Under typical

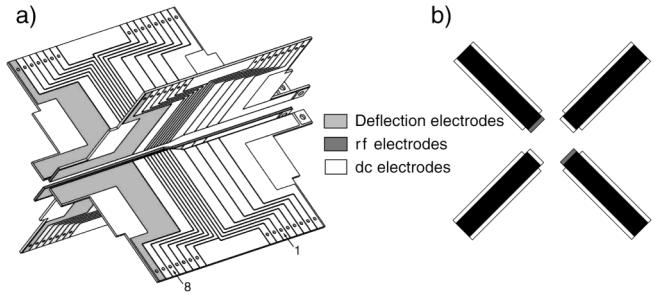

FIG. 1. (a) Sketch of the segmented linear Paul trap with dc electrodes (white) and rf electrodes (dark grey). Deflection electrodes (light gray) are used to alter the trajectories of ions which are extracted out of the trap. (b) Front view showing that rf and rf-ground electrodes (generating the radial confinement) are only covering the two 410 μm wide front faces of the blades.

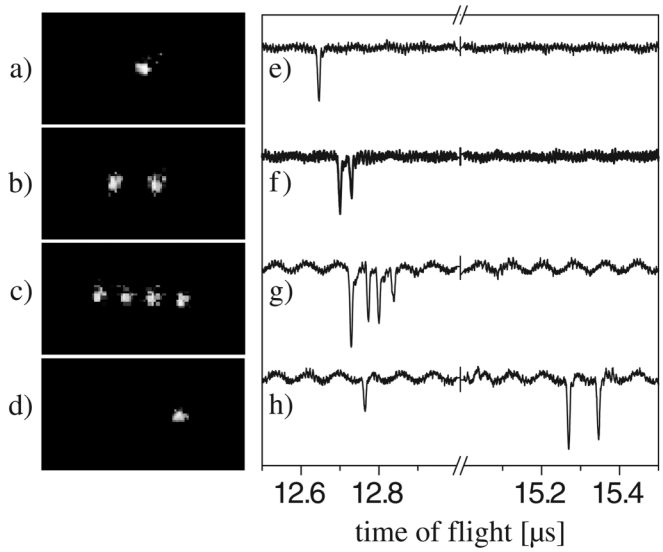

FIG. 2. Typical fluorescence image of a single $^{40}Ca^{+}$ ion (a), and linear ion crystals of two (b) and four (c) ions. After the extraction we record EMT detector signal traces with a single-ion detection event (e), two events (f) and four events (g), correspondingly. The EMCCD image (d) shows fluorescence from a single $^{40}Ca^{+}$ ion only; however, we can discover from its position that it is trapped in a linear crystal together with two dark ions at the left-hand side. As the mixed ion crystal is extracted, we detect three events, one from the $^{40}Ca^{+}$ near 12.8 μs and two events near 15.3 μs. From this time-of-flight spectroscopy, we reveal the mass of CaO^{+} ions for both dark ions. All measurements were conducted without the movable aperture plate with an effective distance of 247 mm between trap center and detector.

operating conditions we apply to the rf electrodes an amplitude of 200 V at the frequency of $\Omega/2\pi = 12.155$ MHz leading to a radial secular frequency $\omega_{\text{rad.}}/2\pi = 430$ kHz for a $^{40}Ca^{+}$ ion. The dc-electrode trap segments 2 and 8 are supplied with 35 V and the remaining electrodes with 0 V resulting in an axial potential with $\omega_{\text{ax.}}/2\pi = 280$ kHz. The location of trapped ions is above electrode 5. The trap assembly is housed in a stainless steel vacuum chamber with enhanced optical access held by a turbomolecular pump and an ion-getter pump at a pressure of 3×10^{-9} mbar. Ions are illuminated by resonant laser light near 397 and 866 nm for Doppler cooling. Scattered photons are collected by a $f/1.76$ lens on a EMCCD camera to image individual $^{40}Ca^{+}$ ions; see Figs. 2(a)–2(c). From the width of the laser excitation spectrum on the $S_{1/2}$-$P_{1/2}$ laser cooling transition, we deduce a temperature of about 2 mK slightly above the Doppler cooling limit.

Calcium and dopant ions are generated in a multiphoton ionization process by a pulsed frequency tripled Nd-YAG laser at 355 nm with a pulse power of 7 mJ. Dopant ions are sympathetically cooled and identified from the voids in the fluorescence image compared to that of a regular linear $^{40}Ca^{+}$ crystal. Figure 2(d) shows the fluorescence of an ion crystal consisting of a single $^{40}Ca^{+}$ and two molecular CaO^{+} ions resulting from a chemical reaction with background residual gas [18]. We identify the species of dark ions by exciting collective vibrational modes with an ac voltage applied to electrode 4 and observing a blurring of the $^{40}Ca^{+}$ fluorescence image at the resonance frequency $\omega_{\text{ax.}}$ [19]. Alternatively, amplitude modulated resonant laser light is used [18] to determine the charge to mass ratio of trapped particles at a precision of better than 0.2%. Before extraction, the sympathetically cooled doping ions may be separated from the $^{40}Ca^{+}$ ions. This is achieved by converting the axial trapping potential into a double well. The doping ions are further transported away from the $^{40}Ca^{+}$ ions by time dependent dc-electrode voltages [21]. As heating generated during this separation process [17] cannot be cooled away anymore an alternative separation method would deflect the unwanted $^{40}Ca^{+}$ ions after extraction, e.g., by increasing the electrode voltages of an einzel-lens. For the extraction we increase the dc voltage of segments 4 and 5 to 500 V within a few tens of nanoseconds. The switching of the extraction voltage (supplied by iseg inc., Model EHQ-8010p) is performed by two high voltage switches (Behlke inc., HTS 41-06-GSM) triggered via a computer-controlled TTL signal and synchronized with the rf-field phase. Synchronization is crucial in order to minimize shot to shot fluctuations of velocity and position. An electronic phase synchronization circuit delays the TTL signal for extraction such that a constant delay to the next zero crossing of the trap drive with frequency Ω is ensured. We found the optimum extraction parameters by matching the time of extraction with a certain phase of the radio frequency and by adjusting the dc voltages on the deflection electrodes, which alter the ion trajectory during extraction. All measurements described below use these settings. The detection of the extracted ions is performed via an electron multiplier tube (EMT) with 20 dynodes from ETP inc., model AF553, which can detect positively charged ions with a specified quantum efficiency of about 80%. The detector is housed in a separate vacuum chamber at a distance of 287 mm from the trap. At typical operating conditions the detector is supplied with a voltage of

-2.5 kV. The gain is specified with 5×10^5 and we observe an electrical signal of about 100 mV. The detection events show a width of 10 to 15 ns. In order to measure the beam divergence a movable aperture plate was installed in front of the detector. This plate, mounted on a nanopositioning stage from Smaract, model SL-2040, features hole diameters ranging from 5 mm down to 300 μm.

Typical EMT detector signals for different numbers of ions are shown in Figs. 2(e)–2(g). Figure 2(h) displays the detector events for one $^{40}Ca^+$ ion and two CaO^+ ions, which arrive at $t = 15.3$ μs. From a time-of-flight analysis through the 1 mm aperture we deduce a mean ion velocity of 19.47 km/s for the $^{40}Ca^+$ ions. At 3×10^{-9} mbar we detect $87(^{+7}_{-11})\%$ of all extracted single ions within a 1σ-confidence interval. We found that the efficiency slightly depends on the residual gas pressure but is mainly limited by the detector efficiency (which we measure to be higher than specified). The measured longitudinal velocity distribution (see Fig. 3) shows a 1σ-spread of 6.3(6) m/s which is about a factor of 10 larger than the velocity distribution inside the trap at $T = 2$ mK. This leads to a relative velocity uncertainty $\Delta v/v$ of 3.2×10^{-4} which may be further reduced by post-accelerating the ions after extraction. From measurements conducted with the smallest aperture (300 μm) we deduce a 1σ-spot radius of $83(^{+8}_{-3})$ μm for the trajectories of the extracted ions. Here we assume a Gaussian spatial distribution and the error is due to counting statistics. Note that this value is an upper limit as our measurements are currently affected by a measured drift of the ion beam of about 15 μm/min possibly caused by temperature drifts of the setup.

For a comparison of measured data with numerical Monte Carlo simulations we need accurate electrostatic potentials which we deduce from a complete CAD-model of the trap geometry created with AUTOCAD. Electrostatic potentials and fields are calculated by using a boundary element method accelerated by the fast multipole method [22]. Symmetry properties of the trap are exploited to reduce numerical errors. The ion trajectories are obtained by applying the Verlet integration method. The initial momentum and position is determined from the thermal Boltzmann distribution in the trapping potential. As a test, we have compared measured trap frequencies $\omega_{\text{ax.}}$ and $\omega_{\text{rad.}}$ for various traps of different size and shape in our lab [23] with corresponding simulations and found an agreement at the level of 2% to 3%. The ion trajectory calculation takes into account the full time dependent dynamics, including the micromotion at frequency Ω yielding a 1σ-velocity spread of 12 m/s and a beam divergence of 130 μrad. Simulated velocity uncertainty and beam divergence agree within 1 order of magnitude with experimental results (see Table I).

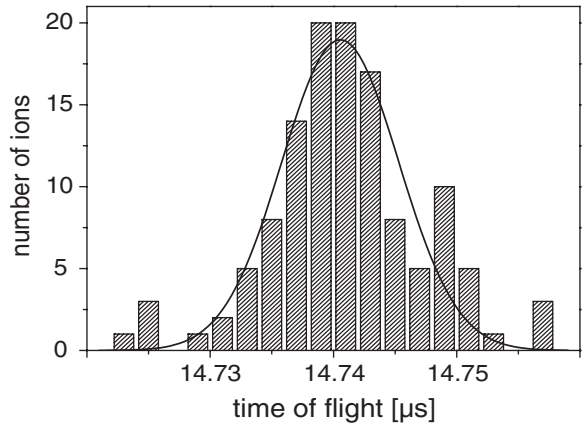

FIG. 3. Time-of-flight distribution for single ions based on 123 successful extractions out of 139 shots in total through the 1 mm aperture. The bin size of the histogram is 2 ns. A Gaussian fit of the data yields an average velocity of 19.47 km/s with a 1σ-spread of 6.3(6)m/s.

In order to implant single ions into solid state materials with nanometer spatial resolution, the detector will be replaced by a simple electrostatic einzel-lens [24] with a diameter of 1 mm and a focal length of 9 mm. Simulations predict a 1σ-spot radius of 7 nm for 2 mK and 2 nm for 100 μK, respectively (see Fig. 4 and Table I).

We attribute the discrepancies between experimental results and numerical simulations to patch electric fields on insulating surfaces, geometrical imperfections of the electrodes and fluctuations of the extraction voltage power supply (specified with $\Delta U/U = 10^{-5}$). The aforementioned drift of the ion beam will be reduced in future experiments by installing magnetic shielding and a temperature stabilization.

Currently, our initial mean spatial and momentum spread is a factor of 10 larger than at the Heisenberg limit. An ideally suited cooling method for reaching this fundamental limit uses the electromagnetically induced transparency, as it allows cooling of all degrees of freedom at different oscillation frequencies even for mixed ion crystals [25,26]. This would lead to the perfect single-ion single-mode matter-wave source. By changing the trapping parameters we can freely adjust the ratio between the variance of the spatial components versus variance of the momentum components.

Thus, the spot size would be limited by the diffraction of the matter wave, which results in a spot size of 10^{-10} m if we assume a numerical aperture of 0.001 for the ion lens and an energy of 80 eV. To assure the proper alignment of a short focal length lens system with respect to the substrate

TABLE I. Comparison between experimental and numerical 1σ-longitudinal velocity uncertainty Δv, beam divergence α (full angle) and 1σ-focal spot radius r_f for different initial ion temperatures T.

	T	Δv	α	r_f
Meas.	2 mK	6.3 m/s	600 μrad	⋯
Calc.	2 mK	12 m/s	130 μrad	7 nm
Calc.	100 μK	1 m/s	30 μrad	2 nm

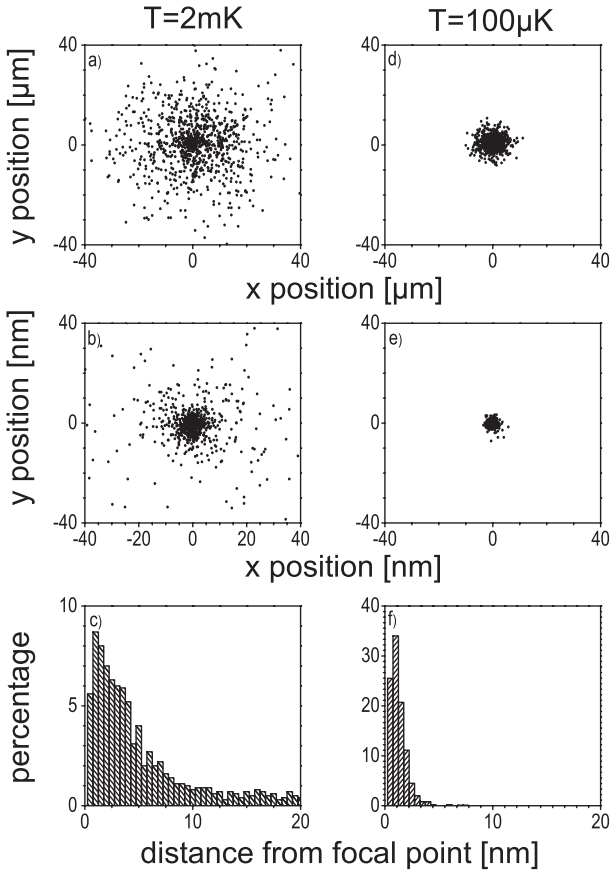

FIG. 4. Monte Carlo simulation of extracted ions. Left side: (a) Spot diagram at a distance of 247 mm from the trap center for an initial ion temperature of 2 mK. (b) Focal spot diagram generated by an einzel-lens with a 1σ-spot radius of 7 nm. (c) Histogram of radial distribution of spots in the focal plane. Right side: (d)–(f) Similar diagrams as on the left side but for a temperature of 100 μK.

we propose to implant through a hole in the tip of an atomic force microscope [27,28]. This would bring along the additional advantage that the charged particle could be placed with respect to surface structures (such as gate electrodes) in deterministic doping applications. A further possible application of our system is as on-demand source for matter-wave interferometry with ultracold slow ions, which until now was only possible with electrons, neutrons, and neutral atoms and molecules [29–32]. Being compatible with state of the art ion trap quantum processors, our setup may be used to convey qubits directly from one trap to the other by transmitting the qubit carrier itself.

In conclusion, we have experimentally realized a deterministic ultracold source for single ions and ionic molecules. For an ion temperature of a few mK we measured a longitudinal velocity distribution of extracted ions which shows a 1σ-spread of a few meters per second which is a promising starting point for the application of ion optical elements. Ion ray tracing simulations predict nm resolution for our setup when combined with an electrostatic einzel-lens. If the ions are further cooled to the motional ground state our setup could realize the perfect matter-wave source at the Heisenberg limit.

We acknowledge financial support by the Landesstiftung Baden-Württemberg in the framework ''atomics'' (Contract No. PN 63.14), the European commission within EMALI (Contract No. MRTN-CT-2006-035369) and the Volkswagen Stiftung.

*kilian.singer@uni-ulm.de
†URL: http://www.quantenbit.de

[1] T. Shinada, S. Okamoto, T. Kobayashi, and I. Ohdomari, Nature (London) **437**, 1128 (2005).
[2] M. V. Gurudev Dutt *et al.*, Science **316**, 1312 (2007).
[3] P. Neumann *et al.*, Science **320**, 1326 (2008).
[4] B. E. Kane, Nature (London) **393**, 133 (1998).
[5] A. D. Greentree, B. A. Fairchild, F. M. Hossain, and S. Prawer, Mater. Today **11**, 22 (2008).
[6] T. Shinada, H. Koyama, C. Hinishita, K. Imamura, and I. Ohdomari, Jpn. J. Appl. Phys. **41**, L287 (2002).
[7] A. Persaud *et al.*, Quant. Info. Proc. **3**, 233 (2004).
[8] M. Mitic *et al.*, Microelectron. Eng. **78**, 279 (2005).
[9] A. Batra *et al.*, Appl. Phys. Lett. **91**, 193502 (2007).
[10] T. Shinada *et al.*, Nanotechnology **19**, 345202 (2008).
[11] J. L. O'Brien *et al.*, Phys. Rev. B **64**, 161401(R) (2001).
[12] S. R. Schofield *et al.*, Phys. Rev. Lett. **91**, 136104 (2003).
[13] F. J. Ruess *et al.*, Nano Lett. **4**, 1969 (2004).
[14] W. Pok *et al.*, IEEE Trans. Nanotechnol. **6**, 213 (2007).
[15] F. J. Ruess *et al.*, Small **3**, 563 (2007).
[16] J. Meijer *et al.*, Appl. Phys. A **83**, 321 (2006).
[17] M. A. Rowe *et al.*, Quantum Inf. Comput. **2**, 257 (2002).
[18] M. Drewsen, A. Mortensen, R. Martinussen, P. Staanum, and J. L. Sørensen, Phys. Rev. Lett. **93**, 243201 (2004).
[19] H. Nägerl *et al.*, Opt. Express **3**, 89 (1998).
[20] Y. Lee *et al.*, J. Vac. Sci. Technol. B **16**, 3367 (1998) reports measurements of a narrow ion velocity distribution in nondeterministic sources with additional velocity filtering. Our measured velocity uncertainty is more than 1 order of magnitude smaller.
[21] G. Huber *et al.*, New J. Phys. **10**, 013004 (2008).
[22] L. Greengard, *The Rapid Evaluation of Potential Fields in Particle Systems* (M.I.T. Press, Cambridge, Massachusetts, 1988).
[23] S. Schulz, U. Poschinger, F. Ziesel, and F. Schmidt-Kaler, New J. Phys. **10**, 045007 (2008).
[24] A. Septier, CERN Report No. 60-39 (1960).
[25] C. F. Roos *et al.*, Phys. Rev. Lett. **85**, 5547 (2000).
[26] F. Schmidt-Kaler *et al.*, Appl. Phys. B **73**, 807 (2001).
[27] A. Persaud *et al.*, Nano Lett. **5**, 1087 (2005).
[28] J. Meijer *et al.*, Appl. Phys. A **91**, 567 (2008).
[29] C. Jönsson, Z. Phys. **161**, 454 (1961).
[30] O. Carnal and J. Mlynek, Phys. Rev. Lett. **66**, 2689 (1991).
[31] M. Arndt *et al.*, Nature (London) **401**, 680 (1999).
[32] H. Rauch, W. Treimer, and U. Bonse, Phys. Lett. A **47**, 369 (1974).